Optical Bloch-mode-induced quasi phase matching of quadratic interactions in one-dimensional photonic crystals

Daniele Faccio, Francesca Bragheri, and Matteo Cherchi

Pirelli Labs, S.p.A.–Optical Innovation, Viale Sarca 222, 20126 Milano, Italy

Received June 26, 2003; revised manuscript received August 28, 2003; accepted September 16, 2003

We examine in detail the quasi-phase-matching process obtained as a stationary modulation of the fundamental field at the band edge of a finite one-dimensional photonic crystal. The treatment is carried out in terms of the structure Bloch waves and fully explains the behavior of second-harmonic generation in the grating. An integrated microstructured AlGaAs mesa waveguide is proposed that gives efficient second-harmonic and difference-frequency generation in virtue of the combined presence of a periodic modulation of the fundamental-field amplitude and of the photonic bandgap edge. © 2004 Optical Society of America

OCIS codes: 190.0190, 130.0130.

1. INTRODUCTION

Optical frequency conversion has achieved much attention since the introduction of lasers as a means to shift the wavelength to regions where amplifying media are not easily available. Both second ($\chi^{(2)}$) and third ($\chi^{(3)}$) order material nonlinearities have been exploited in this sense: The latter has a much smaller magnitude, but four-wave mixing is not as limited by the phase mismatch, $\Delta\beta = \beta(\Sigma_i \omega_i) - \Sigma_i \beta(\omega_i)$ [where $\beta(\omega_i)$ is the wave vector at frequency ω_i] between interacting wavelengths. Indeed, in order to achieve efficient $\chi^{(2)}$ interactions, it is necessary to carefully phase match the interaction. Many methods have been proposed for this purpose, e.g., birefringent phase matching,[1,2] periodic inversion or cancelation of the nonlinearity for so-called quasi phase matching,[3,4] form birefringence in multilayered waveguides,[5] and photonic bandgap (PBG) assisted phase matching.[6,7] Most notably, PBG materials that rely on a periodic modification of the waveguide refractive index or geometry have recently attracted much interest. Enhancement of nonlinear mixing processes in a periodic stratified medium was originally proposed by N. Bloembergen *et al.*[8] The role of the grating is that of providing the missing $\Delta\beta$ in the nonlinear interaction: Following the terminology proposed by M. Fejer *et al.*,[9] we shall refer to this process as linear quasi phase matching (linear QPM), as only the linear susceptibility is modulated. Linear QPM is independent of the position of the photonic bandgaps, and, in order to be effective, the grating index contrast must be of the same order of the material dispersion,[10] although Balakin *et al.*[11] demonstrated a strong enhancement of the conversion efficiency if the optimal linear QPM frequency coincides with a band edge. Recent studies of nonlinear processes in one-dimensional gratings[12–14] have also been motivated by the possibility of obtaining a simultaneously phase-matched and enhanced nonlinearity near the photonic bandgap edge.[15] It has been shown[16,17] that this enhancement has mainly two origins: a phase matching (dispersive PM) of the nonlinear process by modification of the phase velocities near the PBG edge[6] and a PBG edge mode-density enhancement corresponding to a modification of the group velocities. In $\chi^{(2)}$ materials, the combination of these two effects may give rise to extremely efficient conversion that may scale up to the sixth power with device length L.[18] Although this process is very appealing, it presents serious technological difficulties if it is to be implemented in an integrated optical waveguide. Here we shall deal with semiconductor III–V materials (AlGaAs), which are particularly interesting for their integration capabilities and extremely high second-order nonlinear coefficient. On the other hand, it has also been demonstrated that dispersive PM requires very high index contrast in order to compensate the large material dispersion at telecom wavelengths (around 1550 nm).[13] An example of such an integrated grating is given by M. Midrio *et al.*,[19] where the high index contrast is obtained by alternating layers of material with air. The main inconvenience with such gratings is related to the tolerance to fabrication errors in the periodicity or duty cycle,[19] which become extremely critical.

Starting from the general form of the Bloch modes in the finite one-dimensional PBG crystal, we give a physical interpretation of the band edge linear QPM interaction, from here on referred to as Bloch-wave QPM (BW-QPM). This allows a deeper understanding of the process, and, with a practical application to an integrated waveguide grating, we highlight some peculiar characteristics.

2. THEORY

Maxwell's equations in the slowly varying envelope approximation, with no absorption and under the assumption that the fundamental wave (FF) remains undepleted (i.e., the fundamental wave E_ω does not depend on z), lead

us, in the particular case of second-harmonic generation (SHG), to the single equation for the second-harmonic (SH) field

$$E_{2\omega}(z) = \text{const} \int_0^L f(z)\chi^{(2)}E_\omega^2 \exp(j\Delta\beta z)\mathrm{d}z, \qquad (1)$$

where $f(z)$ is a generic periodic function that may be expressed as a Fourier series, i.e., $f(z) = \Sigma_{n=-\infty}^{\infty} a_n \times \exp(-jnKz)$ with $K = 2\pi/\Lambda$, where Λ is the multilayer periodicity. Λ may be chosen so that there is a term in the Fourier expansion with $\bar{c}K = \Delta\beta$, i.e., $\Lambda = 2\bar{c}l_c$, where $\bar{c}$ is a constant and gives the QPM order and l_c is the coherence length, defined as $\pi/\Delta\beta$. The total (including both wave-vector and grating terms) phase mismatch will then be zero, and we shall have QPM of order $\bar{c}$. In Fig. 1, we show the solution to Eq. (1) in the case of a highly dispersive material, AlGaAs of 1550 nm. The dot curve shows $|\mathrm{SH}|^2$ for $f(z) =$ constant: In this case, the maximum value of $E_{2\omega}(z)$ is reached at odd multiples of the coherence length. The solid curve is for $f(z) = 1 + \cos(Kz)$ (also shown, rescaled, for reference as a dashed curve) with $K = \pi/l_c$ (first-order QPM): as expected, we recover a steady growth of the SH. We note that the effect of periodically modulating the material nonlinearity or the FF field is completely equivalent. Modulation of the material $\chi^{(2)}$ is typically obtained by periodically poling ferroelectric crystal, whereas a modulation of the FF field is more complicated. For example, in a directional coupler, the field in the second waveguide is given by[20] $E_2(z) = [-jE_1(0)\exp(-j\delta z) \times (\kappa/\sqrt{\kappa^2 + \delta^2})]\sin(\sqrt{\kappa^2 + \delta^2}z)$, where κ is the coupling coefficient between the two waveguides, $\delta = (\beta_1 - \beta_2)/2$, and $\beta_{1,2}$ are the wave vectors of the fields $E_{1,2}$ in the first (input) and second waveguide. However, for reasons that will become apparent further on, we are more interested in another mechanism for periodically modulating E_ω, namely, the use of the Bloch mode in a periodic dielectric structure.

If we consider a material with a periodic modulation of the dielectric permittivity ϵ with periodicity Λ, then

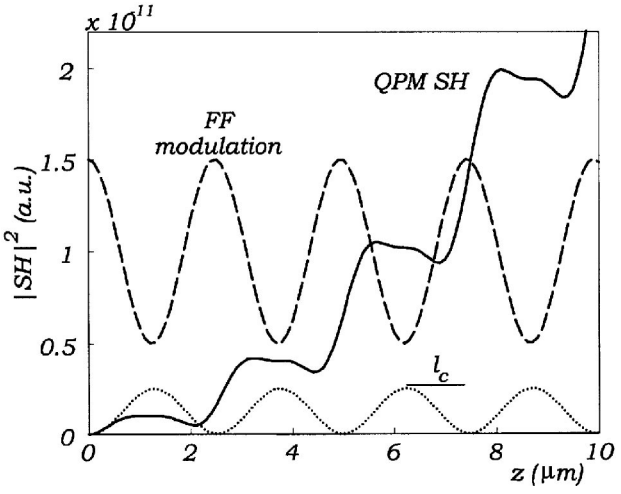

Fig. 1. Numerical solution to Eq. (1) for the non-phase-matched case (dot curve) and for the QPM case (solid curve). The rescaled modulating function is also shown for reference (dashed curve).

Bloch's theorem may be generalized and cites that an electromagnetic wave propagating in this medium may be written as a plane wave, $\exp(j\beta z)$ (where β is the Bloch wave vector and may be easily calculated[21]), modulated by a periodic function $f(z)$ that has the same periodicity of the medium. It is clear that if the Bloch function, defined by the periodicity and amplitude of the refractive-index modulation, is chosen correctly, it will be possible to achieve a QPM nonlinear process obtained by the Bloch-mode modulation of the pump E_ω amplitude.

Let us consider a high-reflectivity, finite, one-dimensional grating. On a transmission peak near the band edge, the grating can be seen as a distributed reflector and, at the same time, as a distributed cavity. As in a Fabry–Perot cavity, the total electric field can be decomposed into a propagating component and a stationary part, which, in turn can be seen as the superposition of a propagating wave and a counterpropagating wave of the same amplitude. The only difference with the Fabry–Perot case is that, due to the distributed nature of the reflectors, power is transferred gradually from the propagating wave to the stationary wave. Furthermore, since the natural modes of the structure are the Bloch modes, the stationary wave E_ω^{staz} must be a superposition of two counterpropagating Bloch modes of the same amplitude. Therefore

$$E_\omega^{\mathrm{staz}} = E_\omega^+ + E_\omega^- = f^+(z)\exp(j\beta z) + f^-(z)\exp(-j\beta z), \qquad (2)$$

where periodic functions may be expressed as Fourier series $f^+(z) = \Sigma_{p=-\infty}^{\infty} a_p \exp(-jpKz)$, and, considering a symmetric structure, $f^-(z) = [f^+(z)]^*$. The Fourier coefficients are complex, so we may put $a_p = \rho_p \exp(j\phi_p)$, and E_ω^{staz} becomes

$$E_\omega^{\mathrm{staz}} = 2\sum_{p=-\infty}^{\infty} \rho_p \cos[(\beta - pK)z + \phi_p]. \qquad (3)$$

We note that the distributed nature of the resonance requires a slow-frequency envelope that can only come from a beating of the terms of the series in Eq. (3). We may combine any two elements $p = n$, m of the sum so that we have

$$E_\omega^{\mathrm{staz}} = 4\cos\left[\left(\beta - \frac{n+m}{2}K\right)z + \psi\right] \times \cos\left(\frac{m-n}{2}Kz + \xi\right), \qquad (4)$$

where $\psi = \psi_m + \psi_n$ and $\xi = \phi_n - \phi_m$. In order for this term to be effective, we must impose resonance conditions on the arguments of the cosine functions. The first condition is

$$\left(\beta - \frac{n+m}{2}K\right)L = t\pi, \qquad (5)$$

where L is the total grating length and t is an integer. Equation (5) requires that the corresponding beating term in Eq. (4) is in resonance with the overall grating structure and bears a close similarity to a Fabry–Perot cavity resonance. Indeed, this resonance arises strictly

from the finite length of the grating, and t gives the order of the transmission resonance.

The second condition is given by the requirement that the standing-wave modulation of the FF field must balance the phase mismatch $\Delta\beta$ of the SH interaction, i.e.,

$$\frac{m-n}{2}K = \bar{c}\Delta\beta, \tag{6}$$

where $\bar{c}$ accounts for the possibility of higher-order QPM. Solving Eqs. (5) and (6) for m and n, we find

$$m = \left[\frac{2n_\omega}{\lambda} - \left(\frac{t}{L} - \frac{\bar{c}}{l_c}\right)\right]\frac{\Lambda}{2},$$

$$n = \left[\frac{2n_\omega}{\lambda} - \left(\frac{t}{L} + \frac{\bar{c}}{l_c}\right)\right]\frac{\Lambda}{2}, \tag{7}$$

where λ is the FF free-space wavelength. These two equations allow us to design a grating for SHG that has a Bloch-wave modulation of the FF field that compensates for the material-dispersion-induced phase mismatch with the FF wavelength simultaneously positioned at a band edge. As an example, we may consider AlGaAs with $l_c = 1.045\,\mu$m, $n_\omega = 3.04$, $L = 500\,\mu$m, and $\lambda = 1.585\,\mu$m. If $t = 1$ (λ is positioned at the first transmission next to a PBG) and $\bar{c} = 1$ (first-order QPM), this leads to $m = 5$, $n = 3$ if the grating periodicity is chosen to be $\Lambda_0 = 2.09\,\mu$m and the order of the Bragg resonance, counting both reflective (Λ is a multiple of $\lambda/4$) and transmissive (Λ is a multiple of $\lambda/2$) resonances, is $n + m = 8$. We note that we also have solutions for m and n for higher-order QPM. In particular, in the example given, we will have all orders up to $\bar{c} = 4$ corresponding to $m = 8$, $n = 0$: These higher-order contributions will be much weaker than the lowest-order one. We also have a degree of freedom in the choice of Λ, which may be taken as an integer multiple of Λ_0. So with $\Lambda = 4.18\,\mu$m, BW-QPM will occur at the $n + m = 16$ band edge, and the lowest-order QPM will be $\bar{c} = 2$.

Note that, in our example, BW-QPM always requires working on higher-order PBGs that consequently will have a lower band-edge mode density if compared with the fundamental PBG. This drawback may be partly recovered if the unit cell with period Λ of the grating is obtained, not from two $\Lambda/2$ layers, but from a combination of $\lambda/4$ layers. In this case, the PBG at λ will have the highest reflectivity and will therefore also exhibit the highest mode-density enhancement.

3. DISCUSSION

In order to illustrate the BW-QPM process, we chose a mesa waveguide in AlGaAs in which the one-dimensional grating is obtained by lateral corrugation of the waveguide, as in Fig. 2. Vertically, the mesa is formed by a lower-cladding layer with refractive index 3.204 and with a thickness $>4\,\mu$m so as to avoid coupling of the optical mode into the underlying GaAs substrate (not indicated in the figure). The core region is 900 nm thick with index 3.282 covered with upper cladding, 440 nm thick and index 3.256. The surrounding medium is air, and the grating is obtained by periodically modulating the waveguide width from 500 to 700 nm. The AlGaAs crystal has (110) orientation so that SH conversion occurs from the FF TE mode to the SH TM mode. The relative effective indices were calculated with a commercial mode solver[22]: $n_\omega = 2.89$, $n_{2\omega} = 3.41$, and the grating index contrast at the FF and SH is $\delta_\omega = 0.18$ and $\delta_{2\omega} = 0.03$, respectively. The unit cell is formed by six layers with thickness (1136–154–1136–154–1136–462) nm. The coherence length in this structure, as calculated from the waveguide grating dispersion relation, is $l_c = 1.045\,\mu$m, whereas $\Lambda = 4.18\,\mu$m, so, according to Eqs. (7), we can expect BW-QPM at the 16th band edge near 1585 nm. Furthermore, the dimensions of the single layers correspond very closely to multiples of $\lambda/4$ so as to optimize the reflectivity and mode density at the 16th band edge. This can be clearly seen in Fig. 3, where we plot the linear transmission (in dB) against the FF wavelength. The bandgaps are numbered starting from the fundamental gap. In practice, Eqs. (7) provide the initial working values for

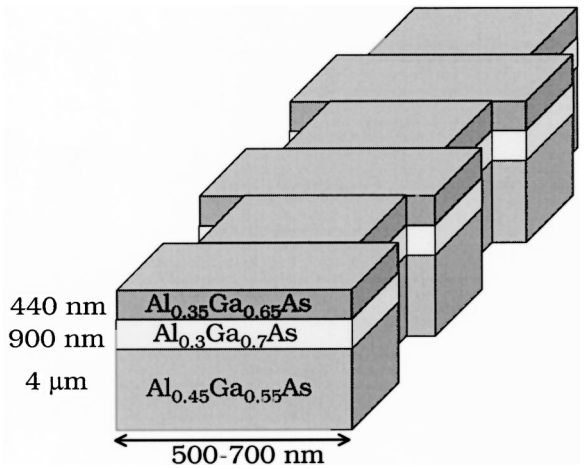

Fig. 2. One-dimensional grating structure realized in a mesa waveguide. All relevant dimensions and Al concentrations are as indicated. The unit cell is formed by six layers with thickness (1136–154–1136–154–1136–462) nm.

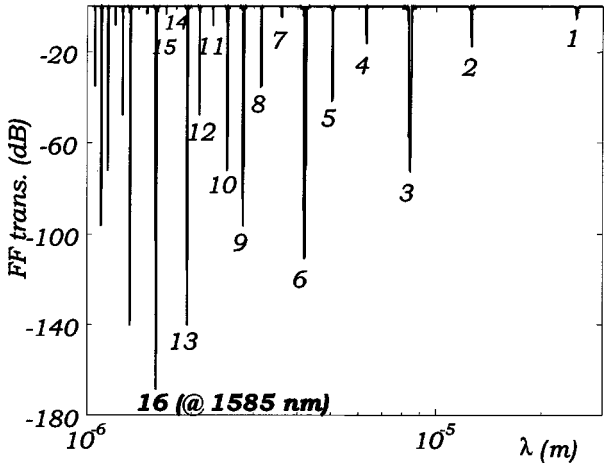

Fig. 3. FF transmission of the 111-unit cell grating. The order of the PBG is indicated in the figure. The reflectivity (and thus the mode density) of the 16th band edge near $\lambda = 1585$ nm has been optimized by use of $\lambda/4$ layers to construct the unit cell, as discussed in the text.

the grating dimensions. A change in the distribution of the layers in the unit cell will cause a small change in the coherence length, which in turn will affect Λ so that the final structure must be fine tuned by a trial and error procedure through computer simulations. We emphasize that the variation of effective index of the FF due to the grating was evaluated around the band edge (1584.9 nm) and was found to be $\Delta n_\omega = 8 \times 10^{-3}$. This maximum value is more than an order of magnitude smaller than material dispersion and is too low to induce phase matching[13]; thus we may exclude the possibility of phase matching by band-edge modification of the effective index. We simulated the linear and nonlinear response of this grating using the transfer-matrix method described in detail elsewhere,[23,24] taking the AlGaAs nonlinearity $\chi^{(2)}_{\mathrm{AlGaAs}} = 100\,\mathrm{pm/V}$ and neglecting pump depletion, which, due to the limited conversion efficiency, proved to be an acceptable approximation. Figure 4(a) shows the linear transmission of the FF field for a grating obtained from 111 unit cells (top graph) along with the SH generated in the forward (middle graph) and backward (bottom graph) directions. The total grating is 463 μm long and is sufficient with a beam area of 1 μm^2 and 50-mW input power to give -23-dB conversion efficiency (10%/W) at the band-edge wavelength 1585.9 nm. In Fig. 4(b) we show the total FF field distribution (top graph) and both the forward and backward SH fields (bottom graph), which clearly illustrates the Bloch-wave resonance in the finite grating and the resulting enhanced mode density for the FF field (the SH field is far from a band edge and does not exhibit mode-density enhancement). To better illustrate the PM mechanism in Fig. 5, we show an enlargement of Fig. 4(b): The top graph shows the total FF field; the Bloch-wave modulation has a periodicity of 4.18 μm. The bottom graph shows the forward-generated SH, which shows local oscillations related to the coherence length; i.e., the Bloch periodicity is 4 times l_c, and we may conclude that the BW-QPM is of second order, as expected. An interesting aspect of this PM technique is the effect of doubling the structure length. At the first transmission peak, we have $t = 1$ in Eqs. (7); if we double L, then, in order to maintain the equality, we must put $t = 2$, i.e., efficient SHG will be observed at the second transmission peak, as can be seen in Fig. 6(a). This may be generalized to longer grating lengths: As L increases, so does the order of the transmission peak at which BW-QPM SHG occurs. Figure 6(b) shows the total squared value of the FF field (top graph) at the second transmission peak. As expected, there are now two main power peaks corresponding to the higher-order Bloch-wave resonance. The forward and backward square-field amplitudes are shown in the bottom graph: The average growth rate with z is quadratic, as is appropriate for QPM SHG and a maximum conversion efficiency of -17-dB (with 50-mW input power) or 40%/W. However, as L, and therefore t, increases, the FF field shifts further away from the band edge, and the mode density will consequently decrease. This results in a SH growth versus L, which becomes nearly linear for large L. This is shown in Fig. 7, where we plot the maximum SHG efficiency for increasing grating lengths.

Finally, the same structure may also be used for difference-frequency generation. In this process, a pho-

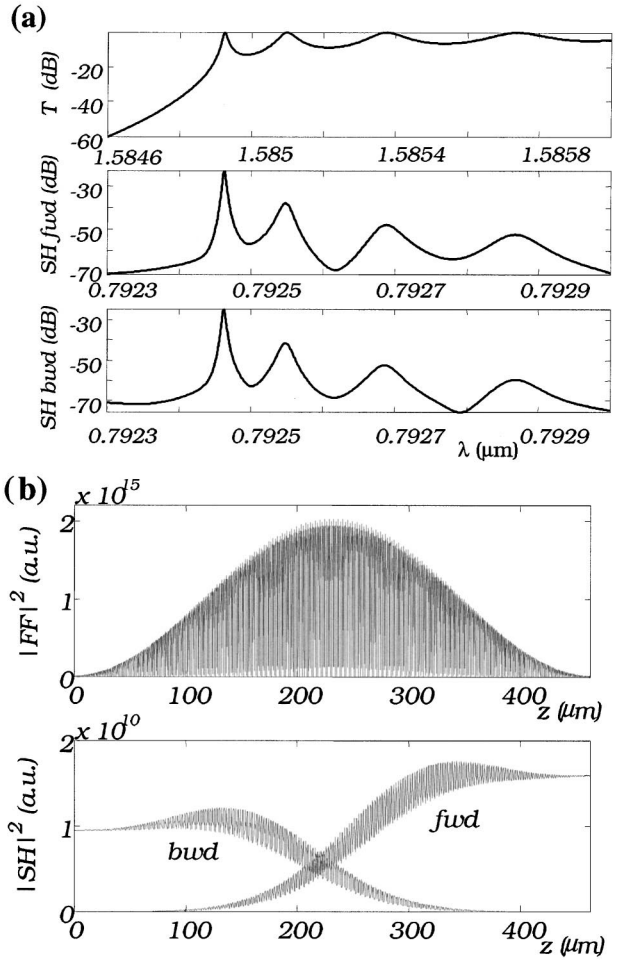

Fig. 4. (a) Top graph: linear transmission of the FF field near the band edge. Middle and bottom graphs: SH efficiency in the forward and backward directions, respectively, with 111 unit cells and other parameters as indicated in the text. (b) FF (top graph) and SH (bottom graph) fields inside the grating.

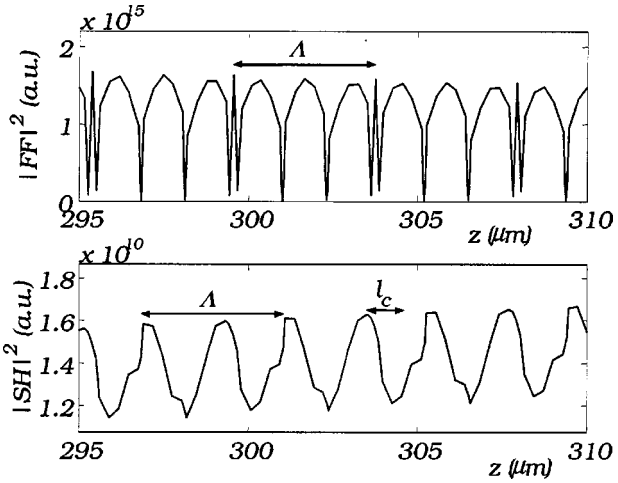

Fig. 5. Enlargement of Fig. 4(b) showing the local field distributions of the FF field (top graph) and SH field (bottom graph) for a grating with 111 unit cells. The Bloch-wave modulation is clearly visible in the FF field, whereas the oscillations in the SH field are related to the coherence length.

ton at frequency ω_s (signal) is converted by a QPM $\chi^{(2)}$ interaction with a photon at frequency ω_p (pump) to a photon at ω_i (idler). Figure 8 shows the calculated conversion efficiency from the fixed input signal wavelength

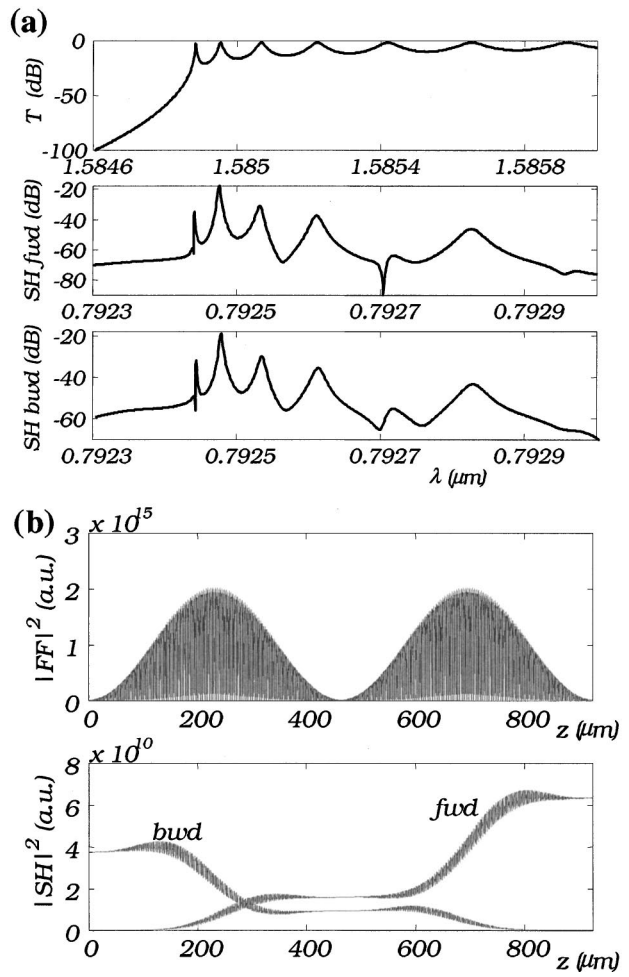

Fig. 6. (a) Top graph: linear transmission of the FF field near the band edge. Middle and bottom graphs: SH efficiency in the forward and backward directions, respectively, with 222 unit cells and other parameters as indicated in the text. (b) FF (top graph) and SH (bottom graph) fields inside the grating.

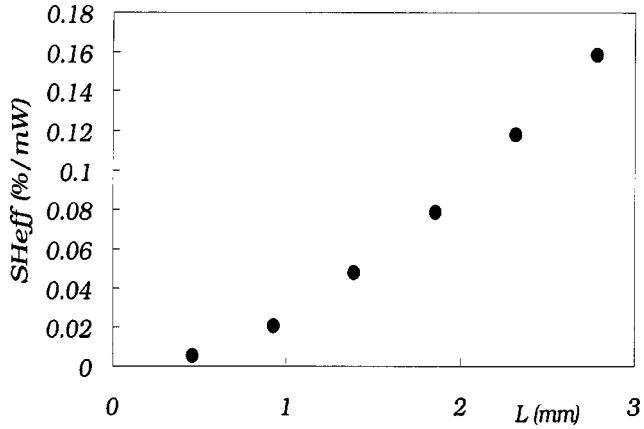

Fig. 7. Maximum SH conversion efficiency in %/mW versus total device length. Each point corresponds to an increase in L of 463 μm, i.e., $L = m \times 463\ \mu$m, and therefore to a shift of the FF peak efficiency to the mth transmission peak from the PBG edge.

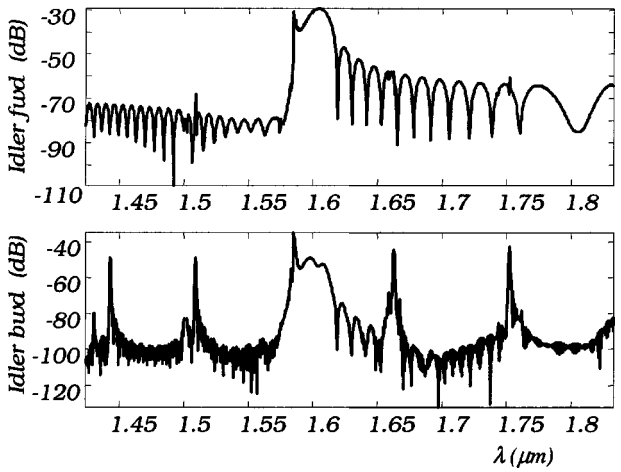

Fig. 8. Idler conversion efficiency versus idler wavelength from the 111-unit cell structure by difference-frequency generation. Signal input power is 1 mW, and the 10-mW pump beam is tuned from 750 to 850 nm.

(1548.9 nm) to the idler for a pump wavelength that is tuned from 750 nm to 850 nm. With 10-mW input pump power and 1-mW input signal power, the 463-μm long structure has −30-dB conversion efficiency with a 13-nm bandwidth. Increasing the length increases the conversion efficiency but also decreases the bandwidth. For example, a 1.7-mm-long grating has −16-dB conversion and a bandwidth of 3 nm.

4. CONCLUSION

In conclusion, we give a description of QPM obtained by periodically modulating the amplitude of the FF field. The modulation is obtained in a linear grating and may be understood in terms of the formation of beating standing-wave Bloch eigenfunctions. This allows an accurate understanding of the linear and nonlinear optical interactions in the multilayer structure, and we have derived simple conditions that define the dimensions of the grating unit cells and layers once the FF wavelength, the coherence, and grating length are given. These conditions impose that the grating compensates for the material phase mismatch at a FF wavelength that is also at PBG edge. The QPM process is usually inefficient so that the enhancement arising from the large mode density at the band edge must be optimized by use of λ/4 layers to construct the unit cell. We also note a peculiar behavior of BW-QPM, namely, the shift of the SH maximum to higher-order FF transmission peaks as the grating length is increased. On the basis of our discussion, we propose an integrated mesa waveguide with a lateral geometric modulation that exhibits efficient SHG and difference-frequency generation. An advantage of using BW-QPM is the lower index contrast required for the grating with respect to "standard" dispersive PM in PBGs. This is important because, although the SH growth versus L is slower with respect to dispersive PM, it allows the use of a wider combination of materials.

This research was partly funded by the European project PICCO.

REFERENCES

1. J. A. Giordmaine, "Mixing of light beams in crystals," Phys. Rev. Lett. **8**, 19–20 (1962).
2. P. D. Maker, R. W. Terhune, M. Nisenhoff, and C. M. Savage, "Effects of dispersion and focusing on the production of optical harmonics," Phys. Rev. Lett. **8**, 21 (1962).
3. S. Somekh and A. Yariv, "Phase matching by periodic modulation of the nonlinear optical properties," Opt. Commun. **6**, 301–304 (1972).
4. C. Conti, G. Assanto, and S. Trillo, "Energy localization through Bragg gratings in quadratic media for second harmonic generation," Acta Phys. Pol. **95**, 719–726 (1999).
5. A. Fiore, V. Berger, E. Rosencher, P. Bravetti, and J. Nagle, "Phase matching using an isotropic nonlinear optical material," Nature **391**, 463–466 (1998).
6. A. Yariv and P. Yeh, "Electromagnetic propagation in periodic stratified media. II. Birefringence, phase matching, and x-ray lasers," J. Opt. Soc. Am. **67**, 438–448 (1977).
7. F. Ranieri, Y. Dumeige, A. Levenson, and X. Letartre, "Nonlinear decoupled FDTD code: phase-matching in 2D defective photonic crystal," Electron. Lett. **38**, 1704–1706 (2002).
8. N. Bloembergen and A. J. Sievers, "Nonlinear properties of laminar structures," Appl. Phys. Lett. **17**, 483–486 (1970).
9. M. M. Fejer, G. A. Magel, D. H. Jundt, and R. L. Byer, "Quasi-phase-matched second harmonic generation: tuning and tolerances," IEEE J. Quantum Electron. **278**, 2631–2654 (1992).
10. C. L. Tang and P. P. Bey, "Phase matching in second harmonic generation using artificial periodic structures," IEEE J. Quantum Electron. **9**, 9–17 (1973).
11. A. V. Balakin, V. A. Bushuev, B. I. Mantsyzov, I. A. Ozheredov, E. V. Petrov, and A. P. Shkurinov, "Enhancement of sum frequency generation near the photonic band gap edge under the quasiphase matching conditions," Phys. Rev. E **63**, 046609 (2001).
12. A. V. Balakin, V. A. Bushuev, N. I. Koroteev, B. I. Mantsyzov, I. A. Ozheredov, A. P. Shkurinov, D. Boucher, and P. Masselin, "Enhancement of second harmonic generation with femtosecond laser pulses near the photonic band edge for different polarizations of incident light," Opt. Lett. **24**, 793–795 (1999).
13. Y. Dumeige, P. Vidakovic, S. Savauge, I. Sagnes, J. A. Levenson, C. Sibilia, M. Centini, G. D'Aguanno, and M. Scalora, "Enhancement of second harmonic generation in a one-dimensional semiconductor photonic band gap," Appl. Phys. Lett. **78**, 3021–3023 (2001).
14. C. Conti, G. Assanto, and S. Trillo, "Cavityless oscillation through backward quasiphase-matched second-harmonic generation," Opt. Lett. **24**, 1139–1141 (1999).
15. M. Scalora, M. J. Bloemer, A. S. Manka, J. P. Dowling, C. M. Bowden, R. Viswanathan, and J. W. Haus, "Pulsed second harmonic generation on nolinear, one-dimensional, periodic structures," Phys. Rev. A **56**, 3166–3174 (1997).
16. J. W. Haus, R. Viswanathan, M. Scalora, A. G. Kalocsai, J. D. Cole, and J. Theimer, "Enhanced second-harmonic generation in media with weak periodicity," Phys. Rev. A **57**, 2120–2128 (1998).
17. M. Centini, C. Sibilia, M. Scalora, G. D'Aguanno, M. Bertolotti, M. J. Bloemer, C. M. Bowden, and I. Nefedov, "Dispersive properties of finite, one-dimensional photonic band gap structures: applications to nonlinear quadratic interactions," Phys. Rev. E **60**, 4891–4898 (1999).
18. Y. Dumeige, I. Sagnes, P. Monnier, P. Vidakovic, C. Meriadec, and A. Levenson, "$\chi^{(2)}$ semiconductor photonic crystals," J. Opt. Soc. Am. B **9**, 2094–2101 (2002).
19. M. Midrio, L. Socci, and M. Romagnoli, "Frequency conversion in one-dimensional stratified media with quadratic nonlinearity," J. Opt. Soc. Am. B **19**, 83–88 (2002).
20. H. A. Haus, *Waves and Fields in Optoelectronics* (Prentice-Hall, Englewood Cliffs, N.J., 1984).
21. P. St. J. Russell, T. A. Birks, and F. D. Lloyd-Lucas, "Photonic Bloch waves and photonic band gaps," in *Confined Electrons and Photons*, E. Burstein and C. Weisbuch (Plenum, New York, 1995), pp. 585–633.
22. Fimmwave, PhotonDesign Ltd, UK.
23. D. S. Bethune, "Optical harmonic generation and mixing in multilayer media: analysis using optical transfer matrix techniques," J. Opt. Soc. Am. B **6**, 910–916 (1989).
24. Y. Jeong and B. Lee, "Matrix analysis for layered quasi-phase-matched media considering multiple reflection and pump wave depletion," IEEE J. Quantum Electron. **35**, 162–172 (1999).